Electronic Supplementary Information (ESI):

High surface area flower-like Ni-Fe layered double hydroxide for electrocatalytic water oxidation reaction

Li-Jing Zhou,[a,‡] Xiaoxi Huang,[b,‡] Hui Chen,[a] Panpan Jin,[a] Guo-Dong Li*[,a] and Xiaoxin Zou*[,a]

a State Key Laboratory of Inorganic Synthesis and Preparative Chemistry, International Joint Research Laboratory of Nano-Micro Architecture Chemistry, College of Chemistry, Jilin University, Changchun 130012, China

b Department of Chemistry and Chemical Biology, Rutgers, The State University of New Jersey, Piscataway, New Jersey, 08854, USA

‡ These authors contributed equally to this work.

*E-mail: X. X. Zou, xxzou@jlu.edu.cn; chemistryzouxx@gmail.com;

G. D. Li, lgd@jlu.edu.cn;

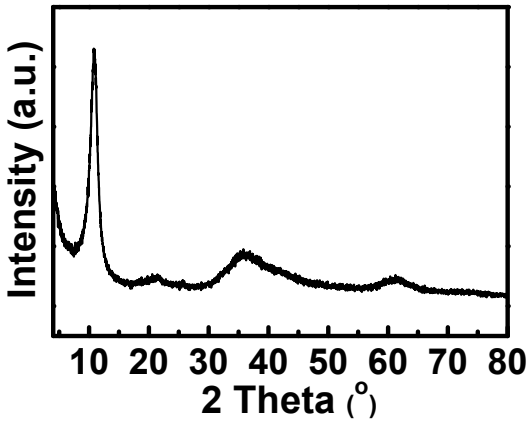

Fig. S1. XRD pattern of the s-NiA material.

Fig. S2. SEM image of the s-NiA.

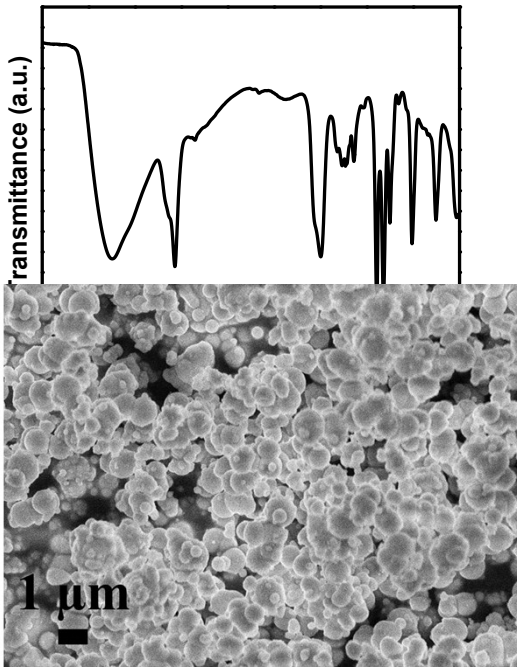

Fig. S3. FTIR spectrum of the s-NiA material.

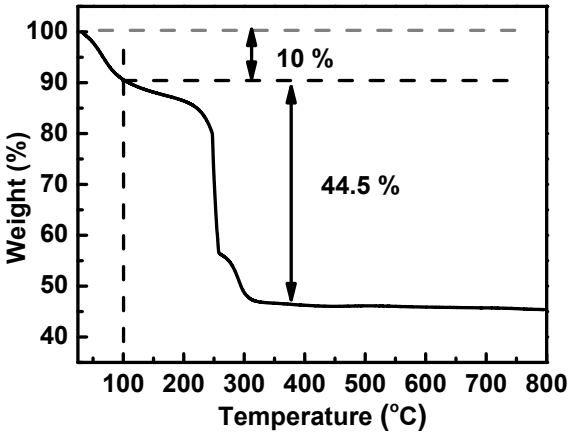

Fig. S4. TGA curve of the sample s-NiA measured in air.

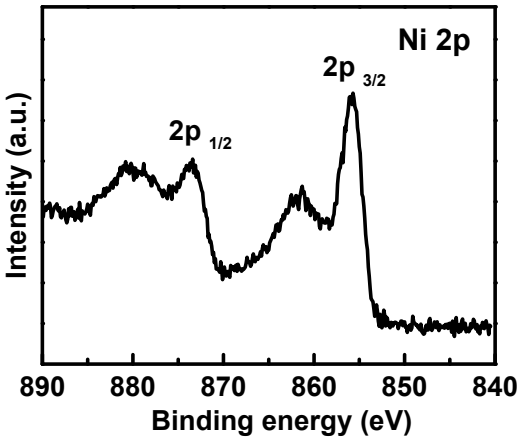

Fig. S5. High-resolution XPS spectra of Ni2p for s-NiA.

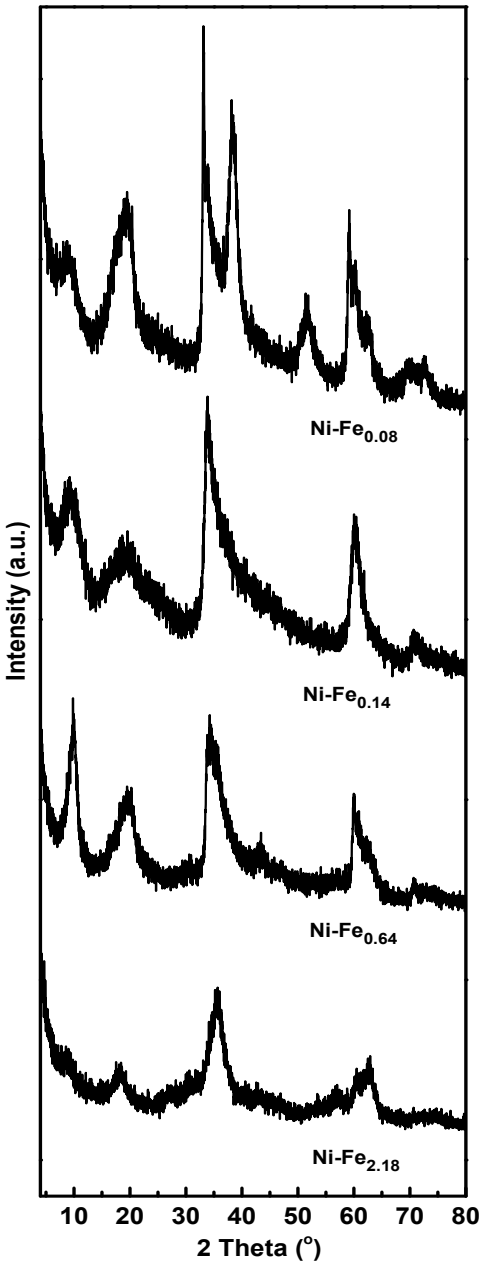

Fig. S6. XRD patterns of Ni-$Fe_{0.08}$, Ni-$Fe_{0.14}$, Ni-$Fe_{0.64}$, Ni-$Fe_{2.18}$ from top to bottom.

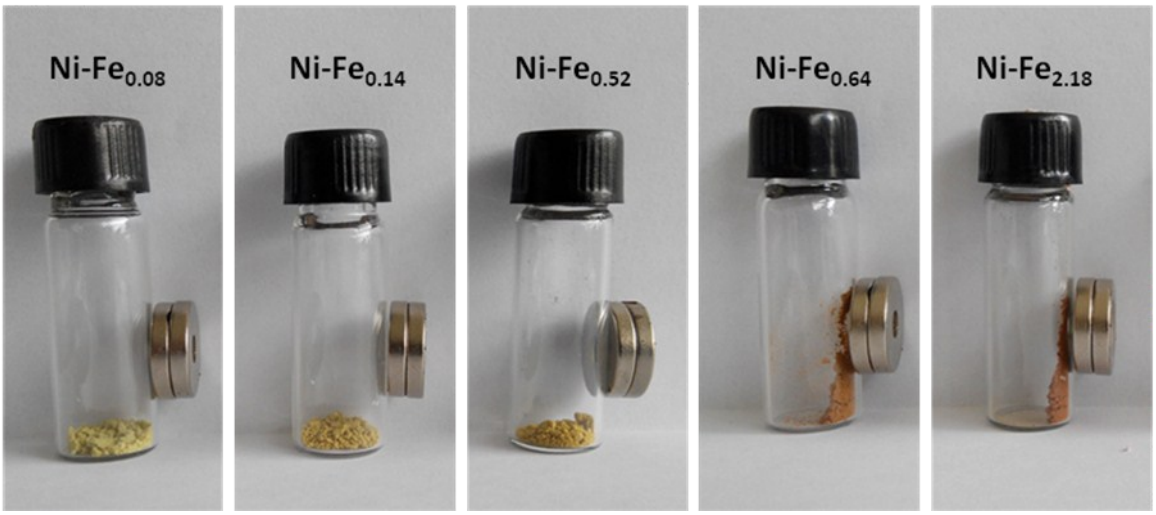

Fig. S7. Digital images of different samples in the presence of magnets.

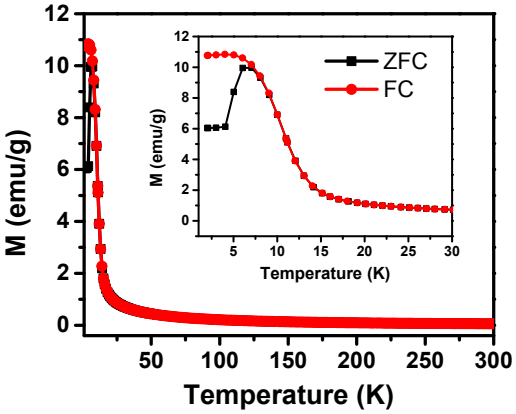

Fig. S8. Temperature dependence of ZFC and FC magnetzation normalized by the sample mass of Ni-$Fe_{0.52}$, the inset shows the enlarged curves between 2 K to 30 K.

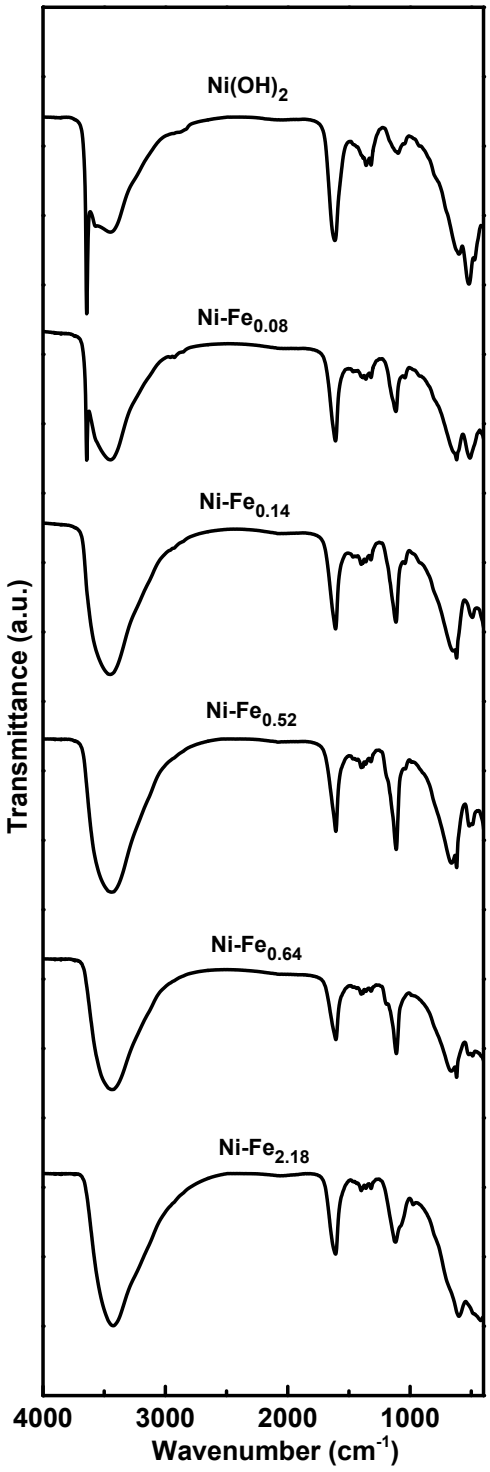

Fig. S9. FTIR spectrums of $Ni(OH)_2$, Ni-$Fe_{0.08}$, Ni-$Fe_{0.14}$, Ni-$Fe_{0.52}$, Ni-$Fe_{0.64}$, Ni-$Fe_{2.18}$ from top to bottom.

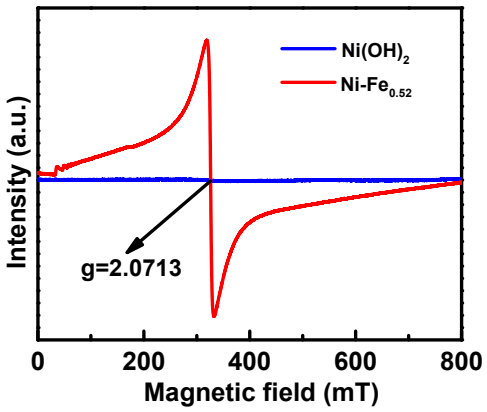

Fig. S10. ESR spectrum of $Ni(OH)_2$ and $Ni\text{-}Fe_{0.52}$ sample.

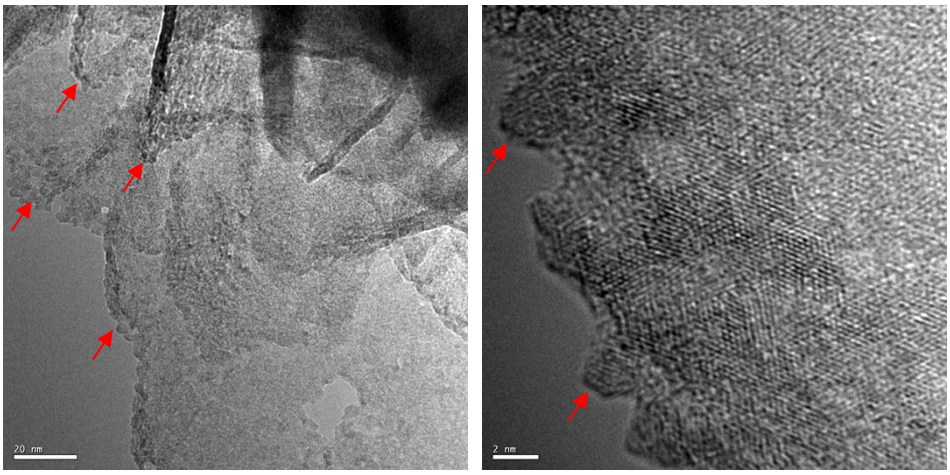

Fig. S11. HRTEM images of $Ni\text{-}Fe_{0.52}$, the red arrows indicate the possible locations of FeO_x species.

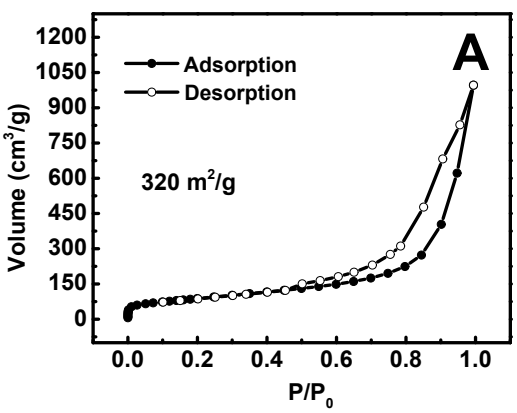
A
Adsorption
Desorption
320 m²/g
Volume (cm³/g)
P/P₀

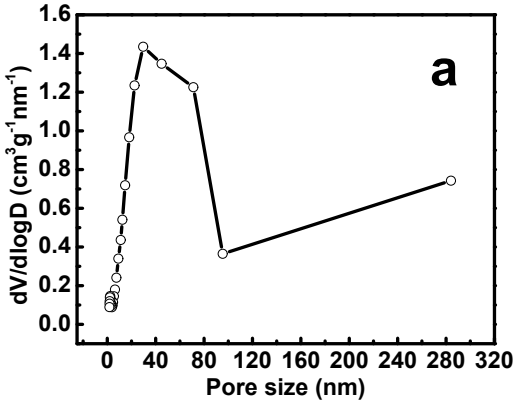
a
dV/dlogD (cm³g⁻¹nm⁻¹)
Pore size (nm)

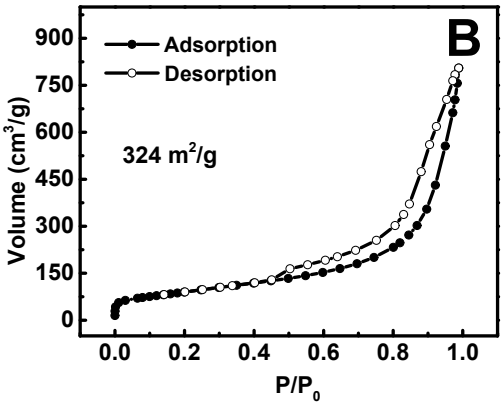
B
Adsorption
Desorption
324 m²/g
Volume (cm³/g)
P/P₀

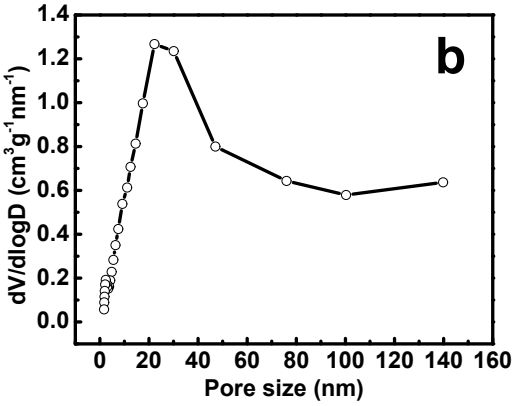
b
dV/dlogD (cm³g⁻¹nm⁻¹)
Pore size (nm)

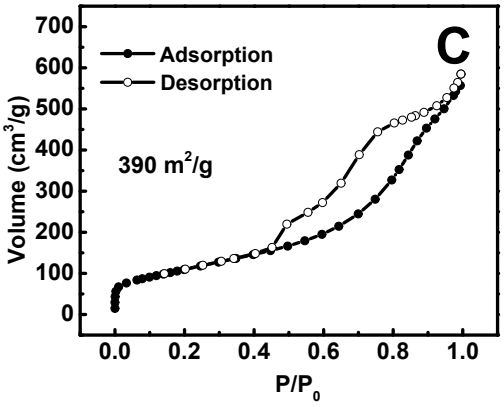
C
Adsorption
Desorption
390 m²/g
Volume (cm³/g)
P/P₀

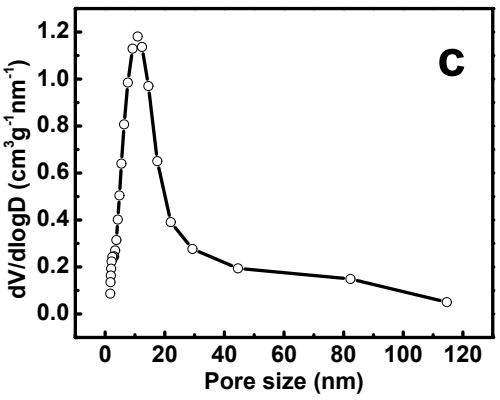
c
dV/dlogD (cm³g⁻¹nm⁻¹)
Pore size (nm)

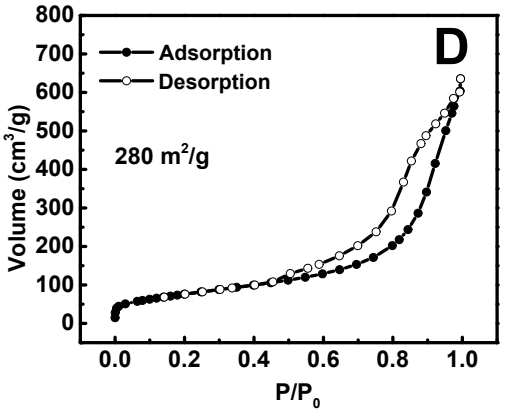
D
Adsorption
Desorption
280 m²/g
Volume (cm³/g)
P/P₀

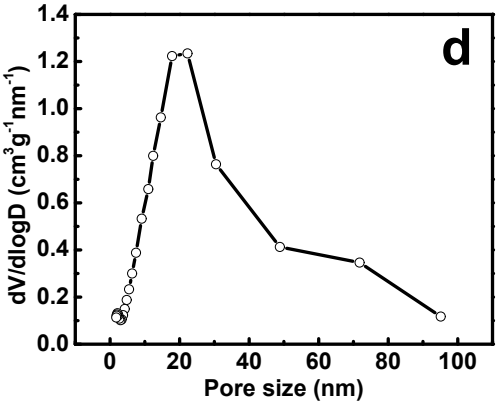
d
dV/dlogD (cm³g⁻¹nm⁻¹)
Pore size (nm)

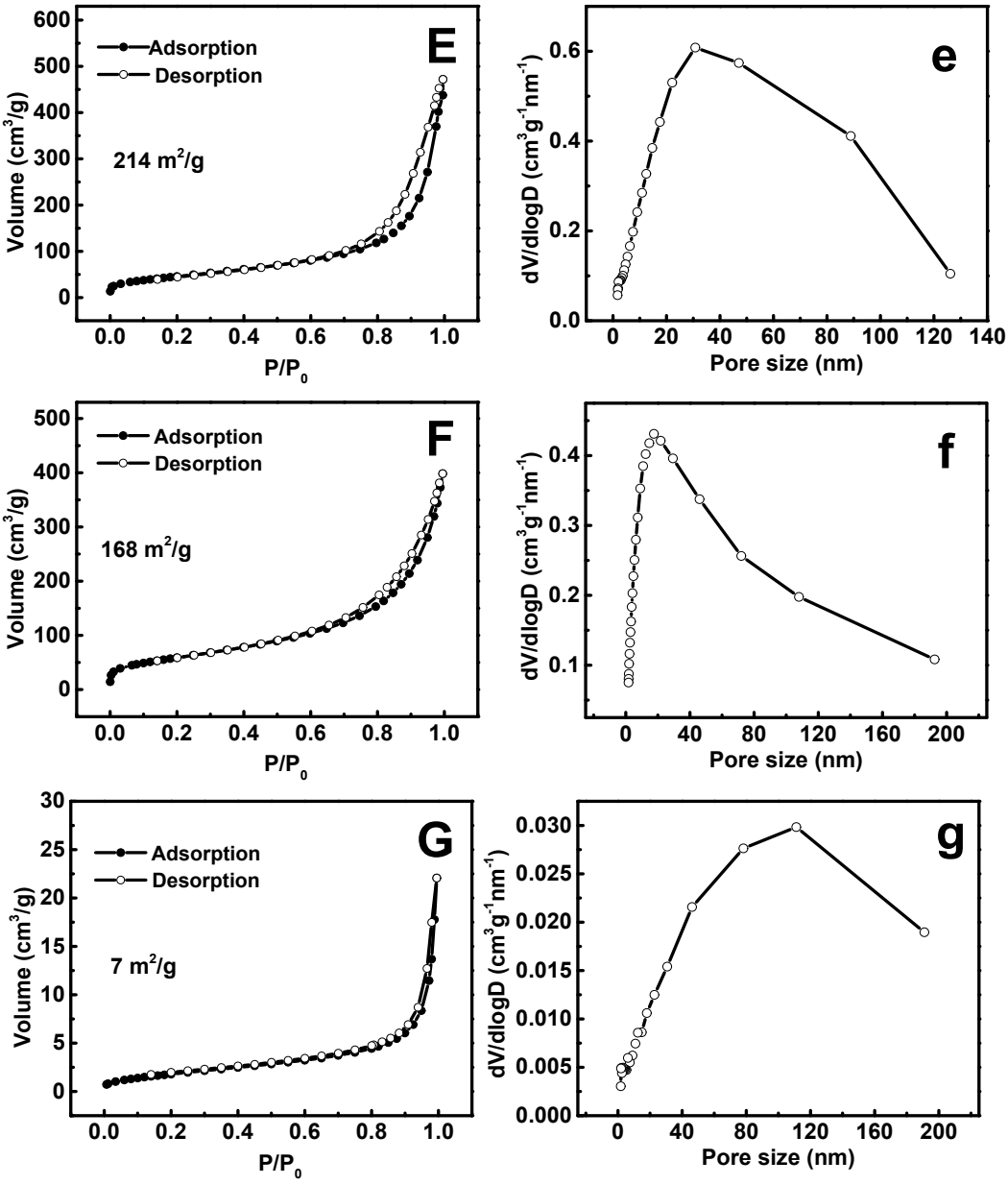

Fig. S12. N_2 adsorption/desorption isotherms of (A) $Ni(OH)_2$, (B) Ni-$Fe_{0.08}$, (C) Ni-$Fe_{0.14}$, (D) Ni-$Fe_{0.52}$, (E) Ni-$Fe_{0.64}$, (F) Ni-$Fe_{2.18}$, (G) α-Fe_2O_3, and the corresponding pore size distribution curve calculated from the adsorption isotherm for (a) $Ni(OH)_2$, (b) Ni-$Fe_{0.08}$, (c) Ni-$Fe_{0.14}$, (d) Ni-$Fe_{0.52}$, (e) Ni-$Fe_{0.64}$, (f) Ni-$Fe_{2.18}$, (g) α-Fe_2O_3. The values in N_2 adsorption/desorption isotherms represent the surface areas of the measured materials with the unit of m^2/g.

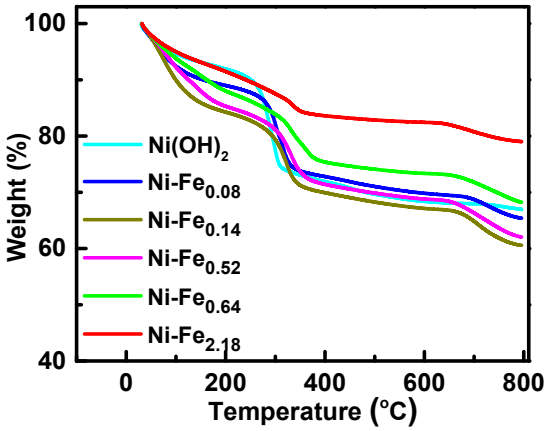

Fig. S13. TGA curves for $Ni(OH)_2$, $Ni\text{-}Fe_{0.08}$, $Ni\text{-}Fe_{0.14}$, $Ni\text{-}Fe_{0.52}$, $Ni\text{-}Fe_{0.64}$, $Ni\text{-}Fe_{2.18}$. The analysis was done in air.

Fig. S14. Molar ratios of Fe:Ni added into the autoclave (black line) for reaction to prepare various $Ni\text{-}Fe_x$ samples, and the corresponding Fe:Ni ratios in the final $Ni\text{-}Fe_x$ material determined by ICP (red line) and XPS (blue line).

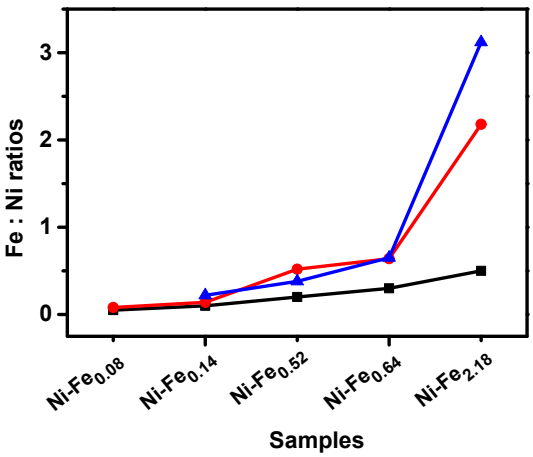

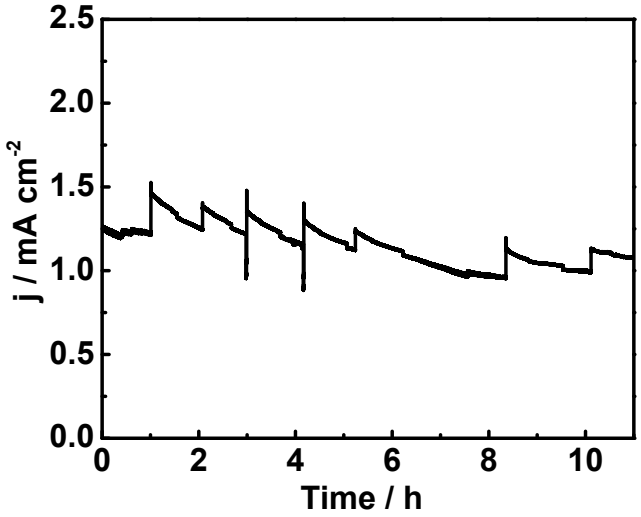

Fig. S15. A current-time curve for Ni-$Fe_{0.52}$ for 11 hours under the potential of 1.47 V vs. RHE.

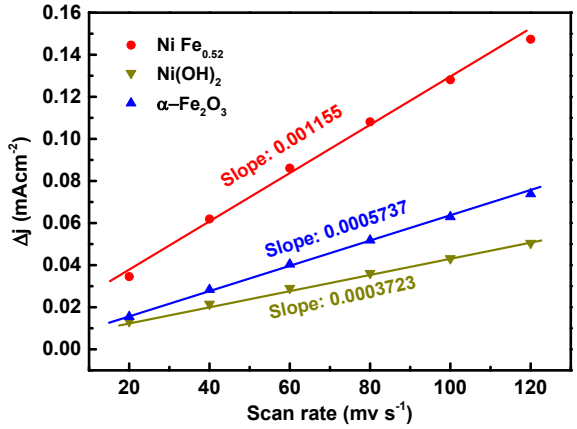

Fig. S16. Charging current density differences plotted against the scan rate for Ni-$Fe_{0.52}$, $Ni(OH)_2$, α-Fe_2O_3. The twice of the double layer capacitance C_{dl}, equivalent to the slope of the linear curve, can be used to estimate the ECSA.

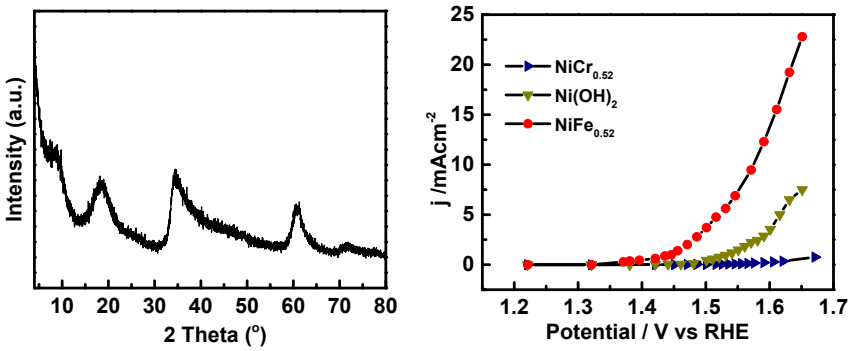

Fig. S17. (left) XRD pattern of Ni-$Cr_{0.52}$; and (right) the comparison of the catalytic activity of Ni-$Cr_{0.52}$, Ni-$Fe_{0.52}$ and $Ni(OH)_2$.

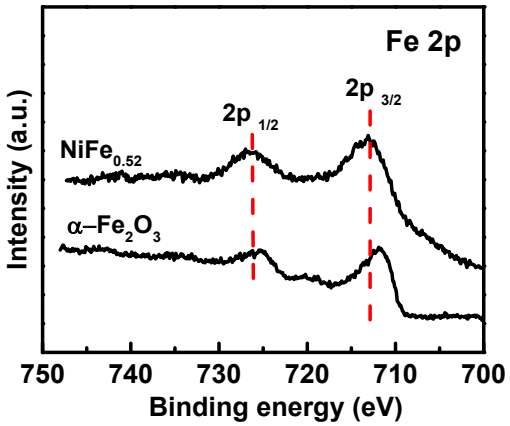

Fig. S18. The comparison of the Fe2p XPS spectra of Ni-$Fe_{0.52}$ and α-Fe_2O_3.

Table S1. Molar ratios of Fe:Ni added at the beginning for reaction to prepare various Ni-Fe_x samples, and the corresponding Fe:Ni ratios in the final Ni-Fe_x material determined by ICP and XPS.

Sample name	Ratios of (Fe:Ni) added into the reaction	Ratios of (Fe:Ni) in the final material detected by ICP	Ratios of (Fe:Ni) in the final material detected by XPS
Ni-$Fe_{0.08}$	0.5:10	0.8:10	--
Ni-$Fe_{0.14}$	1:10	1.4:10	2.2:10
Ni-$Fe_{0.52}$	2:10	5.2:10	3.8:10
Ni-$Fe_{0.64}$	3:10	6.4:10	6.5:10
Ni-$Fe_{2.18}$	5:10	21.8:10	31.2:10

Table S2. Comparisons of Ni-Fe LDH materials on water oxidation reaction (WOR) activity.

#	Material	Electrolyte	Current Density (mA/cm^2)	Overpotential (mV)	Working Condition	Reference
1	Ni-$Fe_{0.52}$ LDH	1 M KOH	10	344	0.14 mg/cm^2 on GCE to get steady state current	This work
2	FeNi-rGO LDH	1 M KOH	10	210	0.25 mg/cm^2 on Ni foam at 5 mV/s	S1
3	FeNi LDH	1 M KOH	10	232	0.25 mg/cm^2 on Ni foam at 5 mV/s	S1
4	NiFe-LDH/CNT	1 M KOH	10	247	0.2 mg/cm^2 on GCE at 5 mV/s with 1600 rpm	S2
5	NiFe-LDH nanoplates	1 M KOH	10	ca. 320	0.2 mg/cm^2 on GCE at 5 mV/s with 1600 rpm	S2
6	CQD/NiFe LDH	1 M KOH	10	235	0.2 mg/cm^2 on GCE at 5 mV/s with 1600 rpm	S3
7	NiFe LDH	1 M KOH	10	330	0.2 mg/cm^2 on GCE at 5 mV/s with 1600 rpm	S3
8	NiFe-LDH grown on Ni foam	1 M KOH	10	240	1 mV/s	S4
9	NiFe-LDH grown on Ni foam	0.1 M KOH	30	280	--	S5
10	$[Ni_{1-x}Fe_x(OH)_2](NO_3)_y(OH)_{x-y}\cdot n H_2O$	1 M KOH	10	260	0.04 mg on 0.09 cm^2 highly ordered pyrolytic graphite	S6
11	NiFe-LDH bulk	1 M KOH	10	347	0.07 mg/cm^2 on GCE at 5 mV/s	S7
12	NiFe-LDH nanosheet	1 M KOH	10	302	0.07 mg/cm^2 on GCE at 5 mV/s	S7

A lot of parameters should be taken into consideration when we want to compare the electrocatalytic activity for different materials. These factors include but not limited to: 1) the concentration of electrolyte solution (0.1 M KOH or 1 M KOH), for higher concentration, the activity would be higher; 2) the sample loading amount, with more samples on the electrode, the current density

normalized by the geometric surface area of the electrode usually goes larger; 3) the selection of electrode for the sample loading, such as glassy carbon electrode (GCE), Ni foam, carbon fiber paper (CFP), the porous Ni foam can provide more accessible surface area, better contact between the catalysts and reactant, and also assist the electrons transport, release of oxygen product; 4) the scan rate also matters since higher scan rate can result in obvious capacitive current, by measuring the steady state current can eliminate the signal due to the capacitance as well; 5) whether the rotating ring disk electrode is used or not, the rotation of electrode can remove the bubbles generated during the oxygen evolution process efficiently, which can further facilitate the interaction between the catalyst and the electrolyte, resulting a higher current density. From the results summarized in Table S2, we can see that the materials Ni-$Fe_{0.52}$ LDH we prepared possess at least alike activities for WOR compared with the NiFe LDH alone in other works (#5, #7, #11) under relatively similar conditions. However, by coupling LDH with other conductive materials, such as graphene (#2), carbon nanotube (#4), carbon quantum dots (#6), nickel foam (#8, #9), or through the exfoliation to expose more active sites (#12), the WOR activity can be enhanced significantly. It's reported that LDHs are generally unconductive, while the carbon nanotube or graphene demonstrate superior electrical conductivity of 0.17-2×10^5 and ca. 10^6 S/cm, respectively.[S8] Thus, the relatively lower activity of our material could be attributed to its intrinsic poor conductivity.

Reference for supporting information:

S1. X. Long, J. Li, S. Xiao, K. Yan, Z. Wang, H. Chen and S. Yang, *Angew. Chem. Int. Ed.*, 2014, **53**, 7584-7588.

S2. M. Gong, Y. Li, H. Wang, Y. Liang, J. Z. Wu, J. Zhou, J. Wang, T. Regier, F. Wei and H. Dai, *J. Am. Chem. Soc.*, 2013, **135**, 8452-8455.

S3. D. Tang, J. Liu, X. Wu, R. Liu, X. Han, Y. Han, H. Huang, Y. Liu and Z. Kang, *ACS Appl. Mate. Interfaces*, 2014, **6**, 7918-7925.

S4. J. Luo, J. H. Im, M. T. Mayer, M. Schreier, M. K. Nazeeruddin, N. G. Park, S. D. Tilley, H. J. Fan, M. Grätzel, *Science*, 2014, **345**, 1593-1596.

S5. Z. Lu, W. Xu, W. Zhu, Q. Yang, X. Lei, J. Liu, Y. Li, X. Sun and X. Duan, *Chem. Commun.*, 2014, **50**, 6479-6482.

S6. B. M. Hunter, J. D. Blakemore, M. Deimund, H. B. Gray, J. R. Winkler and A. M. Müller, *J. Am. Chem. Soc.*, 2014, **136**, 13118-13121.

S7. F. Song, X. Hu, *Nat. Commun.*, 2014, **5**, 4477.

S8. M. Q. Zhao, Q. Zhang, J. Q. Huang, F. Wei, *Adv. Funct. Mater.*, 2011, **22**, 675-694.